

---

# ThermalGen: Style-Disentangled Flow-Based Generative Models for RGB-to-Thermal Image Translation

---

**Jiuhong Xiao**  
 New York University  
 jx1190@nyu.edu

**Roshan Nayak**  
 New York University  
 rn2588@nyu.edu

**Ning Zhang**  
 Technology Innovation Institute  
 ning.zhang@tii.ae

**Daniel Tortei**  
 Technology Innovation Institute  
 daniel.tortei@hotmail.com

**Giuseppe Loianno**  
 University of California, Berkeley  
 loiannog@berkeley.edu

## Abstract

Paired RGB-thermal data is crucial for visual-thermal sensor fusion and cross-modality tasks, including important applications such as multi-modal image alignment and retrieval. However, the scarcity of synchronized and calibrated RGB-thermal image pairs presents a major obstacle to progress in these areas. To overcome this challenge, RGB-to-Thermal (RGB-T) image translation has emerged as a promising solution, enabling the synthesis of thermal images from abundant RGB datasets for training purposes. In this study, we propose **ThermalGen**, an adaptive flow-based generative model for RGB-T image translation, incorporating an RGB image conditioning architecture and a style-disentangled mechanism. To support large-scale training, we curated eight public satellite-aerial, aerial, and ground RGB-T paired datasets, and introduced three new large-scale satellite-aerial RGB-T datasets—**DJI-day**, **Bosonplus-day**, and **Bosonplus-night**—captured across diverse times, sensor types, and geographic regions. Extensive evaluations across multiple RGB-T benchmarks demonstrate that ThermalGen achieves comparable or superior translation performance compared to existing GAN-based and diffusion-based methods. To our knowledge, ThermalGen is the first RGB-T image translation model capable of synthesizing thermal images that reflect significant variations in viewpoints, sensor characteristics, and environmental conditions. Project page: [xjh19971.github.io/ThermalGen](https://xjh19971.github.io/ThermalGen)

## 1 Introduction

Visual-thermal sensor fusion [1] and cross-modality downstream tasks [29, 50, 57, 58, 42] have become increasingly important for integrating visual and thermal data to achieve robust perception under challenging conditions such as low illumination and adverse weather. While deep learning methods [24] have shown promise in these areas, they typically depend on paired RGB-Thermal (RGB-T) data for training. However, such datasets are limited in availability and often difficult to generalize across applications due to domain gaps. Additionally, the cost of collecting synchronized and calibrated RGB-T data is substantial. These limitations motivate the adoption of generative models to synthesize thermal images from RGB inputs as a more scalable and flexible alternative.

Synthesizing thermal data to construct paired RGB-T datasets brings several advantages for cross-modality downstream tasks. First, this method ensures perfectly aligned details between real RGB images and their synthesized thermal counterparts, providing high-quality data for tasks that demand precise cross-modal correspondence, such as dense feature matching [45, 6] and keypoint

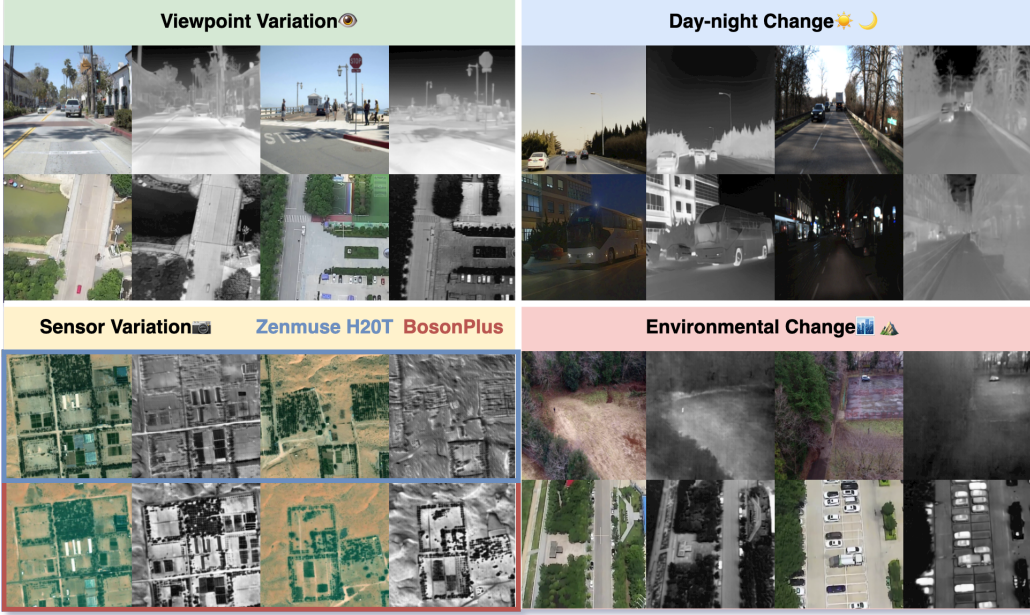


Figure 1: **ThermalGen exhibits robust performance in RGB-to-thermal image translation under diverse conditions.** We present RGB inputs alongside generated thermal images using ThermalGen across a range of challenging variations, including viewpoint variation, day-night change, sensor variation, and environmental change. Variations are illustrated between the two rows in each group.

matching [30]. Second, it enables researchers to exploit the vast repositories of publicly available RGB data, substantially expanding the scale and diversity of training datasets beyond the limited scope of hardware-captured RGB-T pairs, which require specialized calibrated sensors [32, 47] and often suffer from restricted viewpoints [19, 27]. Third, generative models can simulate various thermal characteristics and environmental conditions from a single RGB input, thereby enhancing the robustness of downstream models to variations in thermal sensors and environmental settings.

Benefiting from these advantages, recent studies [57, 58, 56, 50, 20, 12, 10] have demonstrated promising results by leveraging synthesized RGB-T datasets to improve model performance on downstream tasks significantly. In this work, we introduce **an adaptive RGB-to-thermal image translation model** (Fig. 1), aimed at high-fidelity generation across diverse viewpoints, thermal sensors, and environmental factors. The main contributions of this paper are as follows:

- We introduce **ThermalGen**, an adaptive flow-based generative model for RGB-T image translation. Trained on large-scale RGB-T datasets, ThermalGen incorporates an RGB image conditioning architecture with a style-disentangled mechanism, enabling robust generation of thermal images across a wide spectrum of RGB-T styles influenced by thermal sensors, viewpoints, and environmental conditions. The model’s architecture facilitates joint training with additional datasets, promoting adaptability across various applications.
- We release three new satellite-aerial RGB-T paired datasets—**DJI-day**, **Bosonplus-day**, and **Bosonplus-night**—comprising aligned satellite RGB and aerial thermal images with variations in time of day, sensor type, and geographic region. Additionally, we curate an extensive collection of public satellite-aerial, aerial, and ground RGB-T datasets to establish a comprehensive benchmark for large-scale training and evaluation.
- Extensive experiments validate ThermalGen’s effectiveness across multiple benchmarks, demonstrating comparable or superior performance against both GAN- and diffusion-based baselines. We present comprehensive quantitative metrics and qualitative analyses that illustrate the visual fidelity and style embedding influence of our approach. To our knowledge, ThermalGen represents the first model capable of generating high-fidelity thermal imagery across diverse sensor types, viewpoints, and environmental conditions.

## 2 Related Works

**Synthesized Thermal Data for Downstream Tasks.** Recent studies highlight the growing trend of leveraging synthetic thermal data to enhance RGB-T downstream tasks. XoFTR [50] applies randomized cosine transformations to RGB images for improved cross-modal alignment. MINIMA [20] introduces a versatile data engine generating paired datasets across multiple modalities. MatchAnything [12] synthesizes various modalities from inputs like videos and multi-view images for generalizable alignment. AVIID [10] uses synthetic aerial thermal data for object detection, while STGL [57] and STHN [58, 56] boost satellite-thermal retrieval and homography estimation through synthetic RGB-T datasets. These efforts highlight thermal image synthesis as a practical solution to paired data scarcity. In this work, we propose an RGB-T image translation model for general-purpose use, offering broad applicability across diverse downstream tasks.

**RGB-Thermal Image Translation.** Thermal image synthesis from RGB inputs can be formulated as an RGB-T image translation task—an inherently complex problem due to three primary challenges. First, the limited availability of calibrated RGB-T datasets hinders the performance of supervised learning. Unsupervised approaches, such as CycleGAN [63], also struggle to bridge this gap [25]. Second, RGB images inherently lack thermal information, requiring the model to infer thermal cues solely from semantic content. Third, inconsistencies in thermal sensors and camera viewpoints introduce a considerable gap between training and testing distributions [19].

Earlier works [52, 19, 25, 21, 10, 26] primarily used GAN-based approaches [9] to synthesize photorealistic thermal images, while recent studies [62, 38, 35] explore diffusion-based methods for higher fidelity. However, these works are mostly limited by narrow training datasets, reducing generalization across diverse distributions. DiffV2IR [38] is a notable exception, combining public datasets to train a semantic- or text-guided diffusion model. Our work differs in two key ways: (1) we evaluate across satellite-aerial, aerial, and ground datasets, beyond DiffV2IR’s driving-view-focused evaluation; and (2) our style-disentangled model generates target-style thermal images by conditioning on dataset-specific style embeddings, eliminating the need for retraining as required by DiffV2IR.

**Diffusion- and Flow-based General Image Translation.** The success of diffusion-based [15] and flow-based general image generation [31] has enabled advanced image translation methods like Palette [41] for tasks such as colorization and editing. Latent-space models [39, 4] further improved conditional generation quality, leading to a range of high-performance translation techniques. BBDM [28] models domain transitions via a stochastic Brownian Bridge, while Kwon et al. [23] use contrastive learning on DINOv2 [36] features for content-style fusion. Recent style transfer methods [49, 3, 61, 55, 5] also explore text- and style-image-guided transfer. However, RGB-T image translation poses unique challenges due to fundamental modality differences, which prevent direct weight sharing between RGB and thermal domains. Additionally, effective translation requires learning complex cross-modal relationships across diverse RGB-T datasets. These challenges hinder the applicability of RGB style transfer methods for a robust RGB-T image translation model.

## 3 Methodology

### 3.1 Preliminaries

We adopt a flow-based generative paradigm [31] for thermal image synthesis and provide an overview of their underlying process, following the perspective introduced by the Scalable Interpolate Transformer (SiT) [34]. Let  $\mathbf{z}_0 \sim p(\mathbf{z})$  denote the latent variable from data, in accordance with the latent diffusion paradigm [39], and let  $\epsilon \sim \mathcal{N}(\mathbf{0}, \mathbf{I})$  represent standard Gaussian noise. The diffusion process is formulated as a time-dependent continuous process over  $t \in [0, 1]$ , given by:

$$\mathbf{z}_t = \alpha_t \mathbf{z}_0 + \sigma_t \epsilon. \quad (1)$$

Here,  $\alpha_t$  is a decreasing function with  $\alpha_0 = 1$  and  $\alpha_1 = 0$ , while  $\sigma_t$  is an increasing function such that  $\sigma_0 = 0$  and  $\sigma_1 = 1$ . A simple illustrative example of these schedules is  $\alpha_t = 1 - t$  and  $\sigma_t = t$ , with derivatives  $\dot{\alpha}_t = -1$  and  $\dot{\sigma}_t = 1$ . This process can be modeled using a probability flow Ordinary Differential Equation (ODE):

$$\dot{\mathbf{z}}_t = v(\mathbf{z}_t, t), \quad (2)$$

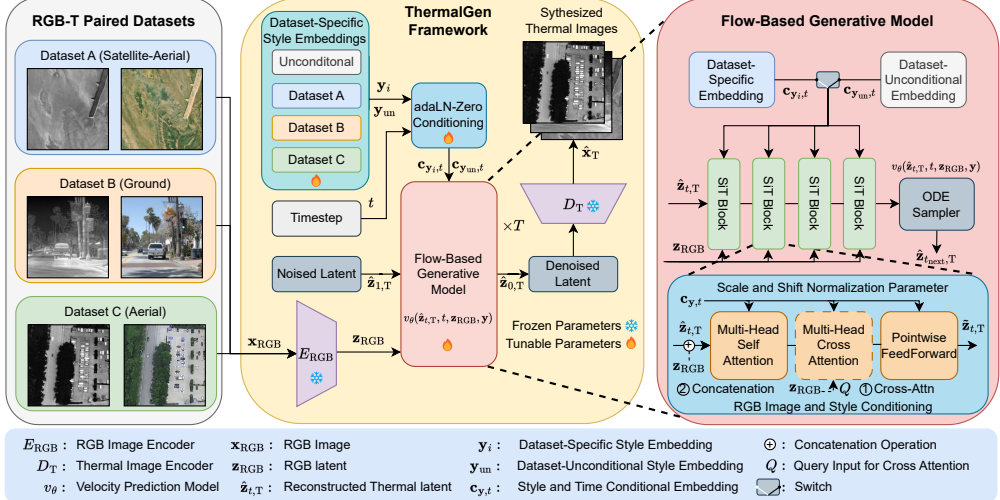


Figure 2: **Overview of ThermalGen.** We sample paired RGB-T data from a diverse collection of satellite-aerial, aerial, and ground datasets for training and evaluation. During thermal image synthesis, the generative model predicts the velocity for  $\hat{\mathbf{z}}_{t,T}$ , conditioned on the timestep  $t$ , the selected dataset-specific style embedding  $\mathbf{y}$ , and RGB latent  $\mathbf{z}_{\text{RGB}}$ . After  $T$  steps of velocity prediction and denoising, the thermal decoder  $D_T$  is used to decode  $\hat{\mathbf{z}}_{0,T}$  and generate the thermal image  $\hat{\mathbf{x}}_T$ .

where  $v$  denotes the velocity function, defined as the expected time derivative of  $\mathbf{z}_t$ :

$$v(\mathbf{z}_t, t) = \mathbb{E}[\dot{\mathbf{z}}_t \mid \mathbf{z}_t = \mathbf{z}] = \dot{\alpha}_t \mathbb{E}[\mathbf{z}_0 \mid \mathbf{z}_t = \mathbf{z}] + \dot{\sigma}_t \mathbb{E}[\epsilon \mid \mathbf{z}_t = \mathbf{z}]. \quad (3)$$

To approximate this velocity function, we employ a neural network  $v_\theta$ , parameterized by  $\theta$ , which is trained by minimizing the following objective:

$$\mathcal{L}_{\text{flow}} = \mathbb{E}_{\mathbf{z}_t, t} \left[ \|v_\theta(\mathbf{z}_t, t) - v(\mathbf{z}_t, t)\|^2 \right]. \quad (4)$$

Once trained, the model can obtain the denoised latent variable  $\hat{\mathbf{z}}_0$  from the terminal noise state  $\mathbf{z}_1 = \epsilon$  by integrating the learned reverse flow dynamics governed by  $v_\theta$ .

### 3.2 RGB-Image-Conditioning and Style-Disentangled Generative Model

The overview of ThermalGen is shown in Fig. 2. Our objective is to synthesize thermal images conditioned on an RGB image and a style embedding disentangled from the model parameters. We define the *RGB-T style* as the mapping relationship between RGB and thermal images, which is influenced by factors such as thermal sensor characteristics, camera viewpoints, and environmental conditions. Let  $p(\mathbf{x}_T)$  denote the distribution of a thermal image  $\mathbf{x}_T \in \mathbb{R}^{H \times W \times 1}$ . ThermalGen models the conditional distribution  $p(\mathbf{x}_T \mid \mathbf{x}_{\text{RGB}}, \mathbf{y})$ , which captures the likelihood of generating  $\mathbf{x}_T$  given an RGB image  $\mathbf{x}_{\text{RGB}} \in \mathbb{R}^{H \times W \times 3}$  and a dataset-specific style embedding  $\mathbf{y} \in \mathbb{R}^{1 \times D}$ . Here,  $H$  and  $W$  refer to the image height and width, and  $D$  denotes the style embedding dimensionality.

**Thermal Image Encoder and Decoder.** To enhance computational efficiency, we adopt the latent diffusion framework [39]. Within this framework, flow and diffusion-based operations are performed on a latent variable  $\mathbf{z}_T = E_T(\mathbf{x}_T)$ , where  $E_T$  is the thermal image encoder. The latent representation  $\mathbf{z}_T \in \mathbb{R}^{\frac{H}{f} \times \frac{W}{f} \times C}$  is a compressed form of the thermal image, with spatial dimensions reduced by a factor of  $f$  and  $C$  representing the number of latent channels. The synthesized thermal image  $\hat{\mathbf{x}}_T$  is reconstructed from the latent variable  $\hat{\mathbf{z}}_T$ , obtained through the flow-based generative model (Section 3.1), using a decoder  $D_T$ , such that  $\hat{\mathbf{x}}_T = D_T(\hat{\mathbf{z}}_T)$ .

**Flow-based Latent Generation.** We employ SiT [34] for flow-based latent generation (Section 3.1), leveraging its scalable diffusion transformer architecture [37]. Let  $v_\theta(\hat{\mathbf{z}}_{t,T}, t, \mathbf{z}_{\text{RGB}}, \mathbf{y})$  denote the velocity predicted by the SiT blocks, conditioned on the noised thermal latent  $\hat{\mathbf{z}}_{t,T}$  at timestep  $t$ , the RGB latent  $\mathbf{z}_{\text{RGB}}$ , and the style embedding  $\mathbf{y}$ . Using the ODE sampler, we update the thermal latent to the next timestep, obtaining  $\hat{\mathbf{z}}_{t+1,T}$ . By iteratively predicting velocities and denoising over  $T$  steps, we progressively reconstruct the thermal latent  $\hat{\mathbf{z}}_{0,T}$  from the initially noised latent  $\hat{\mathbf{z}}_{1,T}$ .

Table 1: **Overview of RGB-T paired datasets.** Sample numbers that correspond to each dataset’s train/validation/test splits are provided. A total of **200k** samples are used for large-scale training. \*For the satellite-aerial datasets, the number of samples is computed using a sample stride of 35m, indicating the gap between adjacent samples.

Dataset Name	Environment	Resolution	Sample Number	Splits	Downstream Tasks
<i>Satellite-Aerial Datasets</i>					
Boson-night* [57]	Wild	512 × 512	13,011/13,011/26,568	train/val/test	Image Alignment
DJI-day* (Ours)	Wild	512 × 512	19,392	train	Image Alignment
Bosonplus-day* (Ours)	Wild	512 × 512	50,882/4,329	train/val	Image Alignment
Bosonplus-night* (Ours)	Wild	512 × 512	50,695/10,146	train/val	Image Alignment
<i>Aerial Datasets</i>					
CalTech [25]	Wild	960 × 600	2,282	train	Semantic Segmentation
LLVIP [19]	Urban	1280 × 1024	12,025/3,463	train/test	Human Detection
NII-CU [44]	Wild	2706 × 1980	2,653/485	train/val	Human Detection
AVIID [10]	Urban	464 × 464	2,412/804	train/test	Object Detection
<i>Ground Datasets</i>					
M <sup>3</sup> FD [32]	Diverse	Diverse	3,360/840	train/test	Object Detection
Freiburg-day [51]	Urban	1920 × 650	12,168/32	train/test	Semantic Segmentation
Freiburg-night [51]	Urban	1920 × 650	8,683/32	train/test	Semantic Segmentation
SMOD-day [2]	Urban	640 × 512	5,378	train	Object Detection
SMOD-night [2]	Urban	640 × 512	3,298	train	Object Detection
MSRS [48]	Urban	640 × 480	1,083/361	train/test	Image Fusion
KAIST [17]	Urban	640 × 512	8,643	train	Human Detection
FLIR [8, 59]	Urban	640 × 512	4,129/1,013	train/test	Object Detection

**Style-Disentangled Mechanism.** To address the diverse RGB-T styles from different datasets, we introduce a style-disentangled mechanism that leverages dataset-specific style embeddings for conditional image generation. We define a set of learnable style embeddings  $Y = \{y_0, y_1, \dots, y_n, y_{un}\}$ , where  $n$  denotes the number of datasets or distinct user-defined RGB-T styles, and  $y_{un}$  represents an unconditional style embedding used for generating thermal images without specifying a style. Given a style embedding  $y_i$  for the  $i^{\text{th}}$  style and a timestep  $t$ , we adopt adaLN-Zero conditioning [37] to generate a corresponding condition embedding  $c_{y_i, t}$ . adaLN-Zero applies adaptive layer normalization, where the scale and shift parameters are modulated based on  $y_i$  and  $t$ . The selection of conditioning methods is motivated by the findings of AdaIN [16], which demonstrated that altering normalization parameters effectively achieves style transfer by modifying feature statistics. For the unconditional style embedding  $y_{un}$ , we denote the resulting condition embedding as  $c_{y_{un}, t}$ . During training, the model randomly selects between  $c_{y_i, t}$  and  $c_{y_{un}, t}$  enabling both Classifier-Free Guidance (CFG) [14] and dataset-unconditional generation. This design allows for straightforward extension to additional datasets by appending new style embeddings, thus enhancing adaptability across varied domains.

**RGB Image Conditioning Architecture.** To incorporate RGB image information into the generative model, we utilize a pretrained KL-VAE encoder [39] as the RGB encoder  $E_{RGB}$ , which extracts the RGB latent representation  $z_{RGB}$ . We explore two variants for RGB image conditioning. ① *Multi-head Cross-Attention (Cross-Attn):* we use  $z_{RGB}$  as the query, while  $\hat{z}_{t, T}$  serves as both the key and value within an additional cross-attention module embedded in the SiT blocks:

$$\tilde{z}_{t, T} = \text{Cross-Attn}(z_{RGB}, \hat{z}_{t, T}, \hat{z}_{t, T}), \quad (5)$$

where  $\tilde{z}_{t, T}$  represents the intermediate features produced by the attention operation. This module is inserted between the self-attention and pointwise feedforward layers in each SiT block. The query-key-value assignment is inspired by style transfer techniques [3, 5], where the content representation serves as the query and the style representation as the key and value. ② *Concatenation:* Alternatively, we can also concatenate  $z_{RGB}$  with  $\hat{z}_{t, T}$  to form the input to the SiT blocks:

$$\bar{z}_{t, T} = \text{Concatenate}(\hat{z}_{t, T}, z_{RGB}), \quad (6)$$

where  $\bar{z}_{t, T}$  denotes the input to the SiT blocks. This method enables convenient fine-tuning from pretrained SiT weights by directly extending the input representations.

## 4 Experiment Setup

**Datasets.** To train a adaptive RGB-T translation model and ensure robust evaluation, we utilize over ten publicly available RGB-T paired datasets, applying a thorough process of curation, filtering, and preprocessing. This includes standardizing data formats, normalizing thermal data to the 8-bit range,

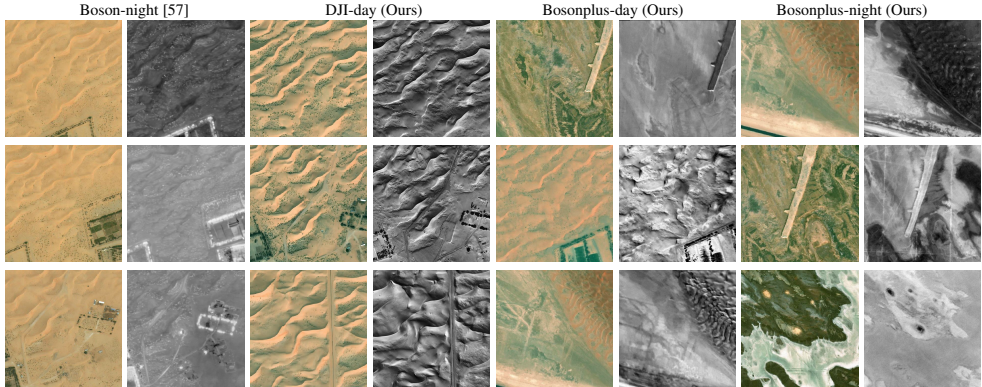


Figure 3: **Visual comparison between the Boson-night dataset [57] and our curated datasets.** Each dataset illustrates differences in thermal sensors, lighting conditions, and geography. Columns show paired satellite RGB and corresponding 8-bit thermal images.

aligning RGB and thermal image pairs, and removing unusable data and regions with invalid thermal readings. Additionally, we introduce three newly collected satellite-aerial RGB-T datasets to enhance translation performance between remote sensing RGB and aerial thermal imagery. A summary of the datasets used is presented in Table 1. The datasets are grouped into three categories: satellite-aerial datasets, aerial datasets, and ground datasets.

**Satellite-Aerial Datasets.** These datasets, such as the Boson-night dataset [57] and our curated datasets—**DJI-day**, **Bosonplus-day**, and **Bosonplus-night** (where the prefix denotes the sensor model and the suffix indicates the time of data acquisition)—comprise paired satellite RGB and aerial thermal images. Details about the data collection process are in Appendix Sec. A. These aligned datasets enable a range of applications, including paired image translation [57], multi-modal image alignment [58, 56], and multi-modal place recognition [57]. A comparison between the Boson-night dataset [57] and our datasets is provided in Appendix Sec. D, highlighting our contributions in terms of broader geographic coverage, increased diversity of thermal sensors, and the inclusion of both daytime and nighttime imagery. Figure 3 offers a visual comparison that illustrates variations across thermal sensors, temporal differences, and the rich geographical diversity captured in our datasets.

**Aerial Datasets.** These datasets include data captured by UAVs or surveillance cameras, featuring oblique aerial views of thermal images. We include four aerial datasets for our training and evaluation: CalTech [25] and NII-CU [44] contain thermal images captured in natural environments, while LLVIP [19] features data from surveillance cameras in the urban or campus environment. Additionally, AVID [10] contains aerial RGB and thermal image pairs collected via a dual-light camera system in an urban environment. Most datasets were collected in daytime settings, though LLVIP and AVID notably include nighttime RGB and thermal data.

**Ground Datasets.** These datasets consist of paired imagery from handheld or vehicle-mounted cameras providing horizontal-view thermal data. We incorporate six datasets for training and evaluation: The M<sup>3</sup>FD dataset [32] delivers RGB-T paired data across varied environments, including urban and wilderness settings, featuring a broad range of objects captured in both daylight and nighttime conditions. The Freiburg [51] and SMOD [2] datasets contribute sequential street-view thermal imagery with day-night change. MSRS [48] provides aligned RGB-T image pairs with high thermal contrast for object detection applications. KAIST Multispectral Pedestrian Detection Benchmark [17] offers regular traffic scenes captured via vehicle-mounted systems for pedestrian detection research. FLIR aligned dataset [59] provides RGB-T paired data from driving scenarios with diverse object classes, including vehicles, pedestrians, and traffic signage.

**Metrics.** We employ four image quality metrics for evaluation: Peak Signal-to-Noise Ratio (PSNR) quantifies image fidelity by measuring the mean-square-error. Structural Similarity Index Measure (SSIM) [54] assesses image structural similarity. Fréchet Inception Distance (FID) [13] measures distribution similarity between predicted and ground truth imagery by comparing 2048-dimensional feature vectors extracted via the Inception v3 model [46]. Learned Perceptual Image Patch Similarity (LPIPS) [60] quantifies perceptual similarity through features from AlexNet [22].

Table 2: **Comparison of RGB-T translation performance on satellite-aerial datasets between baseline methods and ThermalGen.** \*Fine-tuned on M<sup>3</sup>FD; <sup>†</sup>Fine-tuned on FLIR. The best results are in **bold**, and the second and third best are underlined. This is followed in subsequent tables.

Methods	Categories	Boson-night				Bosonplus-day				Bosonplus-night			
		PSNR↑	SSIM↑	FID↓	LPIPS↓	PSNR↑	SSIM↑	FID↓	LPIPS↓	PSNR↑	SSIM↑	FID↓	LPIPS↓
pix2pix [18, 57]	Paired GAN	<u>23.71</u>	<u>0.79</u>	149.55	<u>0.31</u>	<u>14.04</u>	<u>0.30</u>	<u>170.45</u>	<u>0.44</u>	<u>19.93</u>	0.70	137.74	0.40
CycleGAN [63, 12]	Unpaired GAN	17.27	0.50	<u>119.62</u>	0.42	12.62	0.21	279.16	0.52	11.36	0.47	105.36	0.48
pix2pixHD [53]	Paired GAN	21.46	<u>0.75</u>	<u>106.33</u>	<u>0.26</u>	12.85	0.21	<u>157.65</u>	<u>0.43</u>	16.79	0.71	<u>89.26</u>	<u>0.35</u>
VQGAN [7]	Paired GAN	<u>24.55</u>	<u>0.81</u>	207.12	<u>0.29</u>	<u>14.10</u>	<u>0.28</u>	185.41	0.46	<u>18.49</u>	<u>0.76</u>	286.74	<u>0.33</u>
DDIM [39, 43]	Paired Diffusion	18.31	0.72	203.05	0.50	12.50	0.20	261.03	0.71	15.22	<u>0.72</u>	112.38	0.49
BBDM [28]	Paired Diffusion	17.85	0.62	141.27	0.37	12.42	0.18	137.68	0.46	13.88	0.62	101.08	0.43
DiffV2IR [38]	Paired Diffusion	15.47	0.50	150.11	0.47	11.01	0.17	215.20	0.59	13.76	0.55	96.42	0.50
DiffV2IR* [38]	Paired Diffusion	11.69	0.18	253.82	0.66	8.83	0.11	260.42	0.52	10.01	0.25	154.76	0.66
DiffV2IR <sup>†</sup> [38]	Paired Diffusion	15.55	0.46	<u>137.74</u>	0.49	12.32	0.19	234.54	0.56	12.01	0.52	<u>72.02</u>	0.48
ThermalGen-L/2	Paired Diffusion	21.88	0.71	161.22	0.32	<u>14.66</u>	<u>0.31</u>	<u>76.91</u>	<u>0.35</u>	<u>20.47</u>	<u>0.76</u>	<u>75.80</u>	<u>0.34</u>

Table 3: **Comparison of RGB-T translation performance on aerial datasets between baseline methods and ThermalGen.** \*Fine-tuned on M<sup>3</sup>FD; <sup>†</sup>Fine-tuned on FLIR; <sup>‡</sup>DiffV2IR models use LLVIP test set for training.

Methods	Categories	LLVIP				NII-CU				AVIID			
		PSNR↑	SSIM↑	FID↓	LPIPS↓	PSNR↑	SSIM↑	FID↓	LPIPS↓	PSNR↑	SSIM↑	FID↓	LPIPS↓
pix2pix [18, 57]	Paired GAN	<u>12.09</u>	0.37	326.14	0.53	17.31	<u>0.81</u>	168.77	<u>0.37</u>	<u>21.41</u>	<u>0.61</u>	146.26	0.30
CycleGAN [63, 12]	Unpaired GAN	10.39	0.24	227.15	0.61	16.43	0.77	<u>125.37</u>	<u>0.37</u>	15.54	0.46	<u>91.37</u>	0.32
pix2pixHD [53]	Paired GAN	11.51	0.33	281.89	0.51	19.46	0.80	<u>118.60</u>	0.32	20.01	0.56	127.63	0.27
VQGAN [7]	Paired GAN	11.75	0.36	273.06	0.58	<u>15.53</u>	<u>0.81</u>	173.37	0.37	<u>21.71</u>	<u>0.60</u>	96.46	<u>0.23</u>
DDIM [39, 43]	Paired Diffusion	10.94	<u>0.41</u>	297.26	0.71	<u>17.79</u>	0.77	180.14	0.48	10.96	0.36	290.46	0.76
BBDM [28]	Paired Diffusion	9.98	0.22	313.54	0.67	14.36	0.71	<u>118.59</u>	0.42	18.53	0.49	141.06	0.31
DiffV2IR [38]	Paired Diffusion	<u>22.17</u> <sup>†</sup>	<u>0.77</u> <sup>†</sup>	<u>50.10</u> <sup>†</sup>	<u>0.11</u> <sup>†</sup>	12.28	0.63	159.99	0.50	18.17	0.53	<u>51.61</u>	<u>0.21</u>
DiffV2IR* [38]	Paired Diffusion	14.07 <sup>†</sup>	<u>0.51</u> <sup>†</sup>	174.79 <sup>†</sup>	<u>0.46</u> <sup>†</sup>	14.88	0.65	135.15	0.44	14.32	0.45	116.11	0.49
DiffV2IR <sup>‡</sup> [38]	Paired Diffusion	10.23 <sup>†</sup>	0.40 <sup>†</sup>	<u>157.35</u> <sup>†</sup>	<u>0.43</u> <sup>†</sup>	13.76	0.67	132.00	0.44	11.00	0.38	112.97	0.49
ThermalGen-L/2	Paired Diffusion	11.12	0.34	238.60	0.51	<u>26.44</u>	<u>0.92</u>	<u>69.30</u>	<u>0.21</u>	<u>24.89</u>	<u>0.75</u>	<u>29.05</u>	<u>0.13</u>

**Baselines.** We evaluate ThermalGen against widely adopted GAN-based methods for RGB-T image translation [25, 12, 57, 10], including pix2pix [18], CycleGAN [63], pix2pixHD [53], and VQGAN [7]. The pix2pix framework employs a U-Net [40]-based generator and a patch-based discriminator, optimized with L1 loss. In comparison, pix2pixHD adopts ResNet blocks [11] and leverages LPIPS loss [60] to enhance perceptual quality. CycleGAN utilizes two generators and two discriminators to translate images into the target domain and reconstruct them back into the source domain, allowing training on unpaired data. VQGAN incorporates vector quantization with a discrete codebook to improve perceptual quality. For diffusion-based baselines, we compare against DDIM [43] and DiffV2IR [38], all of which employ the latent diffusion model architecture [39] for thermal image generation. All baseline models are trained on our curated RGB-T dataset collection to evaluate cross-dataset generalization, except for DiffV2IR [38], for which we use pretrained models.

**Implementation Details.** For joint training across multiple datasets, we randomly sample batches from all available training sets. During training, each image is randomly resized and cropped to 256 × 256 pixels. For evaluation, images are resized to 256 × 256 pixels with denoising steps  $T = 50$ . The style embedding dimensionality is 1024. Additional training details are in Appendix Sec. C.

## 5 Results

### 5.1 Cross-dataset RGB-T Image Translation Performance

Tables 2-4 present a comprehensive performance comparison between our proposed ThermalGen framework and state-of-the-art baseline methods across representative satellite-aerial, aerial, and ground RGB-T datasets. The results show that ThermalGen outperforms both GAN- and diffusion-based baselines across all categories. In particular, it achieves superior perceptual quality, as measured by FID and LPIPS, on datasets such as Bosonplus-day, Bosonplus-night, NII-CU, AVIID, M<sup>3</sup>FD, and MSRS. The performance advantage is especially notable when compared to fine-tuned DiffV2IR models, which often perform well on isolated datasets but struggle to generalize across diverse imaging conditions. ThermalGen’s robust adaptability stems from its architectural design and unified training strategy, which effectively captures the complex RGB-T patterns in heterogeneous datasets.

### 5.2 Ablation Studies

Figure 4 presents the results of ablation studies conducted to identify the most effective architectural design and hyperparameter configurations for ThermalGen.

Table 4: Comparison of RGB-T translation performance on ground datasets between baseline methods and ThermalGen. \*Fine-tuned on M<sup>3</sup>FD; <sup>+</sup>Fine-tuned on FLIR.

Methods	Categories	M <sup>3</sup> FD				MSRS				FLIR			
		PSNR↑	SSIM↑	FID↓	LPIPS↓	PSNR↑	SSIM↑	FID↓	LPIPS↓	PSNR↑	SSIM↑	FID↓	LPIPS↓
pix2pix [18, 57]	Paired GAN	21.10	0.72	127.62	0.34	21.78	0.68	174.81	0.37	17.13	0.54	224.11	0.44
	Unpaired GAN	11.28	0.42	171.37	0.56	11.42	0.35	99.14	0.53	11.15	0.32	137.97	0.49
	pix2pixHD [53]	19.37	0.67	112.31	0.28	18.21	0.61	121.05	0.35	15.63	0.49	164.53	0.37
VQGAN [7]	Paired GAN	21.02	0.71	79.21	0.26	22.27	0.69	106.51	0.38	16.95	0.50	141.00	0.40
DDIM [39, 43]	Paired Diffusion	11.15	0.45	229.24	0.70	7.35	0.21	262.93	0.79	11.24	0.39	296.81	0.71
BBDM [28]	Paired Diffusion	17.26	0.61	120.79	0.37	20.27	0.62	145.86	0.37	16.10	0.45	177.81	0.42
DiffV2IR [38]	Paired Diffusion	12.24	0.42	75.95	0.45	15.16	0.54	61.52	0.33	20.76	0.52	38.88	0.21
DiffV2IR* [38]	Paired Diffusion	22.76	0.79	37.74	0.13	10.16	0.30	104.01	0.57	11.29	0.44	106.12	0.45
DiffV2IR <sup>+</sup> [38]	Paired Diffusion	12.68	0.45	78.45	0.43	6.80	0.17	113.26	0.64	22.39	0.57	37.83	0.18
ThermalGen-L/2	Paired Diffusion	23.73	0.81	35.82	0.14	24.38	0.76	52.31	0.21	17.10	0.52	70.09	0.33

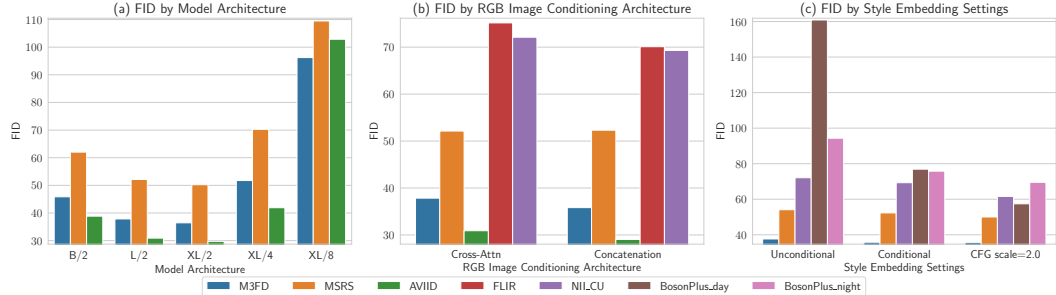


Figure 4: Ablation studies by comparison of FID scores across different model designs.

**Transformer and Patch Sizes.** Figure 4(a) summarizes the performance of RGB-T image translation across various transformer sizes (SiT-B, SiT-L, SiT-XL) and patch sizes (2, 4, 8). The results clearly demonstrate that larger transformer sizes (SiT-L and SiT-XL) outperform the smaller variant (SiT-B) in FID scores across all evaluated datasets (M<sup>3</sup>FD, MSRS, and AVIID). Specifically, SiT-XL/2 achieves the lowest FID scores, indicating superior visual quality and realism. Additionally, models employing smaller patch sizes consistently yield better performance, suggesting that finer granularity for patches substantially enhances the generated image quality.

**RGB Image Conditioning Design.** Figure 4(b) presents an analysis of different configurations for RGB image conditioning, specifically comparing cross-attention and concatenation approaches over five evaluation datasets. The results indicate that concatenating RGB latents yields overall better FID performance than incorporating them as query inputs within the cross-attention module.

**Style Embeddings Settings.** Figure 4(c) evaluates three style embedding configurations: dataset-unconditional style embedding (Unconditional), dataset-specific style embedding (Conditional), and Classifier-Free Guidance (CFG) with scale = 2.0. For datasets with distinctive RGB-T styles (Bosonplus-day, Bosonplus-night, NII-CU), dataset-unconditional style embedding produces degraded FID scores, while CFG (scale = 2.0) outperforms using dataset-specific style embeddings alone. This confirms that style embeddings significantly influence generation quality and encode dataset-specific RGB-T relationships. For general-purpose datasets like M<sup>3</sup>FD and MSRS, the improvement is marginal, likely because these styles are encoded within the generative model.

### 5.3 Qualitative Results

The visualization results in Fig. 6 demonstrate the superior performance of ThermalGen compared to baseline methods across ground, aerial, and satellite-aerial datasets. GAN-based approaches exhibit notable limitations: Pix2Pix and Pix2PixHD generate distorted thermal imagery, while CycleGAN produces outputs resembling grayscale conversions of RGB images, failing to accurately represent thermal distributions. VQGAN results contain prominent grid artifacts that compromise image quality. For diffusion-based methods, DiffV2IR tends to generate thermal images with excessively sharp boundaries, misrepresenting the gradual transitions in actual heat distributions. In contrast, ThermalGen produces high-fidelity thermal images that accurately match the distribution characteristics of ground truth thermal data. This superior performance persists across diverse thermal sensors, viewpoints, and environmental conditions, effectively bridging the substantial domain gaps between satellite-aerial, aerial, and ground-level datasets. In Fig. 7, we observe that our trained DDIM

Table 5: **FID performance across CFG scale factors.** Bold values indicate optimal settings for each dataset.

CFG Scale	Boson-night	FLIR
-	161.22	70.09
2.0	157.57	66.54
4.0	126.50	<b>63.43</b>
8.0	<b>116.46</b>	68.24
16.0	137.95	-

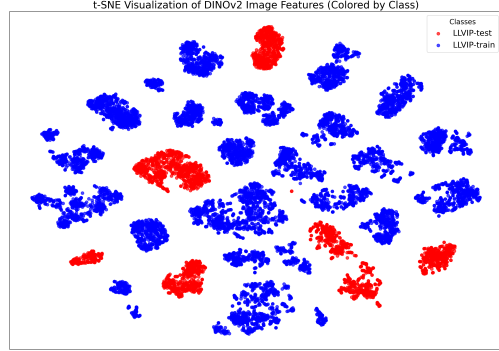


Figure 5: **t-SNE visualization of DINOv2 features for LLVIP thermal images.**

often produces random samples resembling the training distribution rather than being conditioned on the RGB image. This highlights the superior adaptability of ThermalGen compared to DDIM.

#### 5.4 Limitations and Discussions

In Tables 2-4, our results indicate performance degradation in specific datasets, including Boson-night, LLVIP, and FLIR datasets. Through root cause analysis of the visualized outputs and systematic investigation, we identify key limitations and propose targeted solutions for each challenging scenario:

- **Boson-night:** The underperformance stems from extremely low-contrast thermal imagery that hampers effective learning, resulting in dark and blurred outputs. However, this limitation can be effectively mitigated by adjusting the classifier-free guidance (CFG) scale factor. Our analysis in Table 5 reveals that varying the CFG scale significantly impacts generation quality, with an optimal CFG factor of 8.0 reducing the FID from 161.22 to 116.46. This finding underscores the effectiveness of our style embedding mechanism, as the CFG scale controls the influence of style embeddings during generation.
- **FLIR:** Performance issues arise from blurred distant objects and extreme lighting conditions (overexposure and underexposure). Similarly, CFG scale adjustment proves effective in Table 5, with optimal performance achieved at CFG factor 4.0, reducing FID from 70.09 to 63.43. While this does not yet surpass state-of-the-art benchmarks, the consistent trend highlights the potential of our framework to adapt under challenging conditions.
- **LLVIP:** The primary challenge is limited scene diversity with predominantly static backgrounds and minimal dynamic content, creating a distribution shift between training and testing conditions. Through t-SNE analysis of DINOv2 features in Fig. 5, we reveal a clear distribution gap between training and testing thermal images, primarily attributed to camera differences. The most effective solution is expanding the training dataset to bridge this distribution gap and improve generalization.

Overall, these results show that while dataset-specific challenges remain, CFG scale adjustment consistently improves performance and supports the effectiveness of our style-disentangled approach, suggesting promising avenues for further enhancement of cross-domain generalization.

## 6 Conclusions

In summary, we presented **ThermalGen**, an adaptive RGB-Thermal (RGB-T) image translation model built on a flow-based generative architecture with RGB image conditioning and a style-disentangling mechanism. Through extensive experiments on a diverse suite of RGB-T datasets—including three newly introduced satellite-aerial datasets—ThermalGen demonstrates strong cross-dataset generalization across different thermal sensors, viewpoints, and environmental conditions. Our analysis highlights the significance of disentangled style embeddings in enhancing translation robustness.

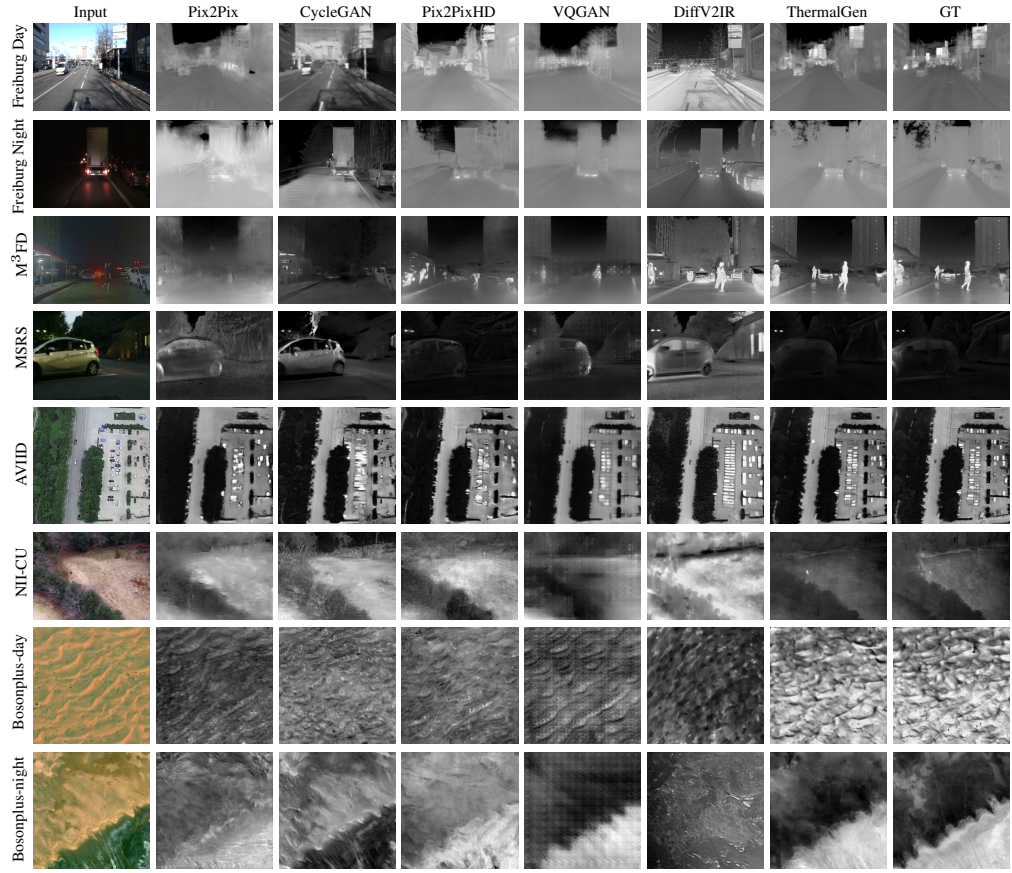


Figure 6: **Visual Comparison of Baseline Methods and ThermalGen.** A comprehensive evaluation is conducted across diverse RGB-T datasets, including ground (Freiburg, M<sup>3</sup>FD, MSRS), aerial (AVIID, NII-CU), and satellite-aerial (Bosonplus-day, Bosonplus-night) domains, demonstrating the method’s adaptability and performance.



Figure 7: **Failure cases of DDIM.** We show paired RGB input and DDIM output. DDIM tends to generate random samples that align with training data, rather than reflecting the RGB input.

Future work will focus on systematically incorporating synthesized thermal data from multiple sources to further advance cross-modal model training.

**Broader Impacts.** ThermalGen generates realistic thermal images from RGB inputs, facilitating the validation of thermal data realism. However, it also presents potential risks of misuse—especially in safety-critical contexts—where synthetic outputs might be misinterpreted as genuine thermal data.

## Acknowledgments

This work was supported by the Technology Innovation Institute, the NSF CAREER Award 2145277, the NSF CPS Grant CNS-2121391, and the NYU IT High Performance Computing resources, services, and staff expertise. We thank the support from Technology Innovation Institute - ARRC - ViCon team. Giuseppe Loianno serves as consultant for the Technology Innovation Institute. This arrangement has been reviewed and approved by the New York University in accordance with its policy on objectivity in research.

## References

- [1] Martin Brenner, Napoleon H Reyes, Teo Susnjak, and Andre LC Barczak. Rgb-d and thermal sensor fusion: A systematic literature review. *IEEE Access*, 11:82410–82442, 2023.
- [2] Zizhao Chen, Yeqiang Qian, Xiaoxiao Yang, Chunxiang Wang, and Ming Yang. Amfd: Distillation via adaptive multimodal fusion for multispectral pedestrian detection. *arXiv preprint arXiv:2405.12944*, 2024.
- [3] Jiwoo Chung, Sangeek Hyun, and Jae-Pil Heo. Style injection in diffusion: A training-free approach for adapting large-scale diffusion models for style transfer. In *Proceedings of the IEEE/CVF conference on computer vision and pattern recognition*, pages 8795–8805, 2024.
- [4] Quan Dao, Hao Phung, Binh Nguyen, and Anh Tran. Flow matching in latent space. *arXiv preprint arXiv:2307.08698*, 2023.
- [5] Yingying Deng, Xiangyu He, Fan Tang, and Weiming Dong. Z\*: Zero-shot style transfer via attention reweighting. In *Proceedings of the IEEE/CVF Conference on Computer Vision and Pattern Recognition*, pages 6934–6944, 2024.
- [6] Johan Edstedt, Qiyu Sun, Georg Bökman, Mårten Wadenbäck, and Michael Felsberg. Roma: Robust dense feature matching. In *Proceedings of the IEEE/CVF Conference on Computer Vision and Pattern Recognition*, pages 19790–19800, 2024.
- [7] Patrick Esser, Robin Rombach, and Bjorn Ommer. Taming transformers for high-resolution image synthesis. In *Proceedings of the IEEE/CVF conference on computer vision and pattern recognition*, pages 12873–12883, 2021.
- [8] TELEDYNE FLIR. Free teledyne flir thermal dataset for algorithm training. <https://www.flir.com/oem/adas/dataset-form/>, 2025. Online; accessed 21 Apr 2025.
- [9] Ian Goodfellow, Jean Pouget-Abadie, Mehdi Mirza, Bing Xu, David Warde-Farley, Sherjil Ozair, Aaron Courville, and Yoshua Bengio. Generative adversarial networks. *Communications of the ACM*, 63(11):139–144, 2020.
- [10] Zonghao Han, Ziye Zhang, Shun Zhang, Ge Zhang, and Shaohui Mei. Aerial visible-to-infrared image translation: Dataset, evaluation, and baseline. *Journal of remote sensing*, 3:0096, 2023.
- [11] Kaiming He, Xiangyu Zhang, Shaoqing Ren, and Jian Sun. Deep residual learning for image recognition. In *IEEE International Conference on Computer Vision and Pattern Recognition (CVPR)*, pages 770–778, 2016.
- [12] Xingyi He, Hao Yu, Sida Peng, Dongli Tan, Zehong Shen, Hujun Bao, and Xiaowei Zhou. Matchanything: Universal cross-modality image matching with large-scale pre-training. *arXiv preprint arXiv:2501.07556*, 2025.
- [13] Martin Heusel, Hubert Ramsauer, Thomas Unterthiner, Bernhard Nessler, and Sepp Hochreiter. Gans trained by a two time-scale update rule converge to a local nash equilibrium. *Advances in neural information processing systems*, 30, 2017.
- [14] Jonathan Ho and Tim Salimans. Classifier-free diffusion guidance. *arXiv preprint arXiv:2207.12598*, 2022.
- [15] Jonathan Ho, Ajay Jain, and Pieter Abbeel. Denoising diffusion probabilistic models. *Advances in neural information processing systems*, 33:6840–6851, 2020.
- [16] Xun Huang and Serge Belongie. Arbitrary style transfer in real-time with adaptive instance normalization. In *Proceedings of the IEEE international conference on computer vision*, pages 1501–1510, 2017.
- [17] Soonmin Hwang, Jaesik Park, Namil Kim, Yukyung Choi, and In So Kweon. Multispectral pedestrian detection: Benchmark dataset and baselines. In *Proceedings of IEEE Conference on Computer Vision and Pattern Recognition (CVPR)*, 2015.
- [18] Phillip Isola, Jun-Yan Zhu, Tinghui Zhou, and Alexei A Efros. Image-to-image translation with conditional adversarial networks. In *IEEE/CVF Conference on Computer Vision and Pattern Recognition (CVPR)*, pages 1125–1134, 2017.
- [19] Xinyu Jia, Chuang Zhu, Minzhen Li, Wenqi Tang, and Wenli Zhou. Llvip: A visible-infrared paired dataset for low-light vision. In *Proceedings of the IEEE/CVF international conference on computer vision*, pages 3496–3504, 2021.

[20] Xingyu Jiang, Jiangwei Ren, Zizhuo Li, Xin Zhou, Dingkang Liang, and Xiang Bai. Minima: Modality invariant image matching. *arXiv preprint arXiv:2412.19412*, 2024.

[21] Vladimir V Kniaz, Vladimir A Knyaz, Jiri Hladuvka, Walter G Kropatsch, and Vladimir Mizginov. Thermalgan: Multimodal color-to-thermal image translation for person re-identification in multispectral dataset. In *Proceedings of the European conference on computer vision (ECCV) workshops*, pages 0–0, 2018.

[22] Alex Krizhevsky, Ilya Sutskever, and Geoffrey E Hinton. Imagenet classification with deep convolutional neural networks. In *Advances in Neural Information Processing Systems*. Curran Associates, Inc., 2012.

[23] Gihyun Kwon and Jong Chul Ye. Diffusion-based image translation using disentangled style and content representation. In *The Eleventh International Conference on Learning Representations*, 2023.

[24] Yann LeCun, Yoshua Bengio, and Geoffrey Hinton. Deep learning. *nature*, 521(7553):436–444, 2015.

[25] Connor Lee, Matthew Anderson, Nikhil Ranganathan, Xingxing Zuo, Kevin Do, Georgia Gkioxari, and Soon-Jo Chung. Caltech aerial rgb-thermal dataset in the wild. In *European Conference on Computer Vision*, pages 236–256. Springer, 2024.

[26] Dong-Guw Lee, Myung-Hwan Jeon, Younggun Cho, and Ayoung Kim. Edge-guided multi-domain rgb-to-tir image translation for training vision tasks with challenging labels. In *2023 IEEE International Conference on Robotics and Automation (ICRA)*, pages 8291–8298, 2023.

[27] Alex Leykin, Yang Ran, and Riad Hammoud. Thermal-visible video fusion for moving target tracking and pedestrian classification. In *2007 IEEE Conference on Computer Vision and Pattern Recognition*, pages 1–8. IEEE, 2007.

[28] Bo Li, Kaitao Xue, Bin Liu, and Yu-Kun Lai. Bbdm: Image-to-image translation with brownian bridge diffusion models. In *Proceedings of the IEEE/CVF conference on computer vision and pattern Recognition*, pages 1952–1961, 2023.

[29] Chenglong Li, Xinyan Liang, Yijuan Lu, Nan Zhao, and Jin Tang. Rgb-t object tracking: Benchmark and baseline. *Pattern Recognition*, 96:106977, 2019.

[30] Philipp Lindenberger, Paul-Edouard Sarlin, and Marc Pollefeys. Lightglue: Local feature matching at light speed. In *Proceedings of the IEEE/CVF International Conference on Computer Vision*, pages 17627–17638, 2023.

[31] Yaron Lipman, Ricky T. Q. Chen, Heli Ben-Hamu, Maximilian Nickel, and Matthew Le. Flow matching for generative modeling. In *The Eleventh International Conference on Learning Representations*, 2023.

[32] Jinyuan Liu, Xin Fan, Zhanbo Huang, Guanyao Wu, Risheng Liu, Wei Zhong, and Zhongxuan Luo. Target-aware dual adversarial learning and a multi-scenario multi-modality benchmark to fuse infrared and visible for object detection. In *Proceedings of the IEEE/CVF conference on computer vision and pattern recognition*, pages 5802–5811, 2022.

[33] Ilya Loshchilov and Frank Hutter. Decoupled weight decay regularization. In *International Conference on Learning Representations*, 2019.

[34] Nanye Ma, Mark Goldstein, Michael S Albergo, Nicholas M Boffi, Eric Vanden-Eijnden, and Saining Xie. Sit: Exploring flow and diffusion-based generative models with scalable interpolant transformers. In *European Conference on Computer Vision*, pages 23–40. Springer, 2024.

[35] Fangyuan Mao, Jilin Mei, Shun Lu, Fuyang Liu, Liang Chen, Fangzhou Zhao, and Yu Hu. Pid: physics-informed diffusion model for infrared image generation. *Pattern Recognition*, 169:111816, 2026.

[36] Maxime Oquab, Timothée Darcet, Théo Moutakanni, Huy Vo, Marc Szafraniec, Vasil Khalidov, Pierre Fernandez, Daniel Haziza, Francisco Massa, Alaeldin El-Nouby, et al. Dinov2: Learning robust visual features without supervision. *arXiv preprint arXiv:2304.07193*, 2023.

[37] William Peebles and Saining Xie. Scalable diffusion models with transformers. In *Proceedings of the IEEE/CVF international conference on computer vision*, pages 4195–4205, 2023.

[38] Lingyan Ran, Lidong Wang, Guangcong Wang, Peng Wang, and Yanning Zhang. Diffv2ir: Visible-to-infrared diffusion model via vision-language understanding. *arXiv preprint arXiv:2503.19012*, 2025.

[39] Robin Rombach, Andreas Blattmann, Dominik Lorenz, Patrick Esser, and Björn Ommer. High-resolution image synthesis with latent diffusion models. In *Proceedings of the IEEE/CVF conference on computer vision and pattern recognition*, pages 10684–10695, 2022.

[40] Olaf Ronneberger, Philipp Fischer, and Thomas Brox. U-net: Convolutional networks for biomedical image segmentation. In *Medical Image Computing and Computer-Assisted Intervention (MICCAI)*, pages 234–241, 2015.

[41] Chitwan Saharia, William Chan, Huiwen Chang, Chris Lee, Jonathan Ho, Tim Salimans, David Fleet, and Mohammad Norouzi. Palette: Image-to-image diffusion models. In *ACM SIGGRAPH 2022 conference proceedings*, pages 1–10, 2022.

[42] Ukcheol Shin, Kyunghyun Lee, In So Kweon, and Jean Oh. Complementary random masking for rgb-thermal semantic segmentation. In *2024 IEEE International Conference on Robotics and Automation (ICRA)*, pages 11110–11117. IEEE, 2024.

[43] Jiaming Song, Chenlin Meng, and Stefano Ermon. Denoising diffusion implicit models. In *International Conference on Learning Representations*, 2021.

[44] Simon Speth, Artur Gonçalves, Bastien Rigault, Satoshi Suzuki, Mondher Bouazizi, Yutaka Matsuo, and Helmut Prendinger. Deep learning with rgb and thermal images onboard a drone for monitoring operations. *Journal of Field Robotics*, 39(6):840–868, 2022.

[45] Jiaming Sun, Zehong Shen, Yuang Wang, Hujun Bao, and Xiaowei Zhou. Loftr: Detector-free local feature matching with transformers. In *Proceedings of the IEEE/CVF conference on computer vision and pattern recognition*, pages 8922–8931, 2021.

[46] Christian Szegedy, Vincent Vanhoucke, Sergey Ioffe, Jon Shlens, and Zbigniew Wojna. Rethinking the inception architecture for computer vision. In *Proceedings of the IEEE conference on computer vision and pattern recognition*, pages 2818–2826, 2016.

[47] Karasawa Takumi, Kohei Watanabe, Qishen Ha, Antonio Tejero-De-Pablos, Yoshitaka Ushiku, and Tatsuya Harada. Multispectral object detection for autonomous vehicles. In *Proceedings of the on Thematic Workshops of ACM Multimedia 2017*, pages 35–43, 2017.

[48] Linfeng Tang, Jiteng Yuan, Hao Zhang, Xingyu Jiang, and Jiayi Ma. Piafusion: A progressive infrared and visible image fusion network based on illumination aware. *Information Fusion*, 83-84:79–92, 2022.

[49] Narek Tumanyan, Michal Geyer, Shai Bagon, and Tali Dekel. Plug-and-play diffusion features for text-driven image-to-image translation. In *Proceedings of the IEEE/CVF Conference on Computer Vision and Pattern Recognition*, pages 1921–1930, 2023.

[50] Önder Tuzcuoğlu, Aybora Köksal, Buğra Sofu, Sinan Kalkan, and A Aydin Alatan. Xoftr: Cross-modal feature matching transformer. In *Proceedings of the IEEE/CVF Conference on Computer Vision and Pattern Recognition*, pages 4275–4286, 2024.

[51] Johan Vertens, Jannik Zürn, and Wolfram Burgard. Heatnet: Bridging the day-night domain gap in semantic segmentation with thermal images. In *2020 IEEE/RSJ International Conference on Intelligent Robots and Systems (IROS)*, pages 8461–8468, 2020.

[52] Emma Wadsworth, Advait Mahajan, Raksha Prasad, and Rajesh Menon. Deep learning for thermal-rgb image-to-image translation. *Infrared Physics & Technology*, 141:105442, 2024.

[53] Ting-Chun Wang, Ming-Yu Liu, Jun-Yan Zhu, Andrew Tao, Jan Kautz, and Bryan Catanzaro. High-resolution image synthesis and semantic manipulation with conditional gans. In *Proceedings of the IEEE Conference on Computer Vision and Pattern Recognition*, 2018.

[54] Zhou Wang, Alan C Bovik, Hamid R Sheikh, and Eero P Simoncelli. Image quality assessment: from error visibility to structural similarity. *IEEE transactions on image processing*, 13(4):600–612, 2004.

[55] Zhizhong Wang, Lei Zhao, and Wei Xing. Stylediffusion: Controllable disentangled style transfer via diffusion models. In *Proceedings of the IEEE/CVF International Conference on Computer Vision*, pages 7677–7689, 2023.

[56] Jiahong Xiao and Giuseppe Loianno. Uasthn: Uncertainty-aware deep homography estimation for uav satellite-thermal geo-localization. In *2025 IEEE International Conference on Robotics and Automation (ICRA)*, pages 14066–14072, 2025.

[57] Jiahong Xiao, Daniel Tortei, Eloy Roura, and Giuseppe Loianno. Long-range uav thermal geo-localization with satellite imagery. In *IEEE/RSJ International Conference on Intelligent Robots and Systems (IROS)*, pages 5820–5827, 2023.

- [58] JiuHong Xiao, Ning Zhang, Daniel Tortei, and Giuseppe Loianno. Sthn: Deep homography estimation for uav thermal geo-localization with satellite imagery. *IEEE Robotics and Automation Letters*, 9(10):8754–8761, 2024.
- [59] Heng Zhang, Elisa Fromont, Sébastien Lefevre, and Bruno Avignon. Multispectral fusion for object detection with cyclic fuse-and-refine blocks. In *2020 IEEE International conference on image processing (ICIP)*, pages 276–280. IEEE, 2020.
- [60] Richard Zhang, Phillip Isola, Alexei A Efros, Eli Shechtman, and Oliver Wang. The unreasonable effectiveness of deep features as a perceptual metric. In *Proceedings of the IEEE conference on computer vision and pattern recognition*, pages 586–595, 2018.
- [61] Yuxin Zhang, Nisha Huang, Fan Tang, Haibin Huang, Chongyang Ma, Weiming Dong, and Changsheng Xu. Inversion-based style transfer with diffusion models. In *Proceedings of the IEEE/CVF conference on computer vision and pattern recognition*, pages 10146–10156, 2023.
- [62] Guoqing Zhu, Honghu Pan, Qiang Wang, Chao Tian, Chao Yang, and Zhenyu He. Data generation scheme for thermal modality with edge-guided adversarial conditional diffusion model. In *Proceedings of the 32nd ACM International Conference on Multimedia*, pages 10544–10553, 2024.
- [63] Jun-Yan Zhu, Taesung Park, Phillip Isola, and Alexei A Efros. Unpaired image-to-image translation using cycle-consistent adversarial networks. In *IEEE International Conference on Computer Vision (ICCV)*, 2017.

## NeurIPS Paper Checklist

### 1. Claims

Question: Do the main claims made in the abstract and introduction accurately reflect the paper's contributions and scope?

Answer: **[Yes]**

Justification: The main claim presented in the abstract and introduction highlights our contributions to a novel RGB-T image translation model, the introduction of new datasets, and our focused scope on RGB-T image translation.

Guidelines:

- The answer NA means that the abstract and introduction do not include the claims made in the paper.
- The abstract and/or introduction should clearly state the claims made, including the contributions made in the paper and important assumptions and limitations. A No or NA answer to this question will not be perceived well by the reviewers.
- The claims made should match theoretical and experimental results, and reflect how much the results can be expected to generalize to other settings.
- It is fine to include aspirational goals as motivation as long as it is clear that these goals are not attained by the paper.

### 2. Limitations

Question: Does the paper discuss the limitations of the work performed by the authors?

Answer: **[Yes]**

Justification: This paper has discussed the limitations.

Guidelines:

- The answer NA means that the paper has no limitation while the answer No means that the paper has limitations, but those are not discussed in the paper.
- The authors are encouraged to create a separate "Limitations" section in their paper.
- The paper should point out any strong assumptions and how robust the results are to violations of these assumptions (e.g., independence assumptions, noiseless settings, model well-specification, asymptotic approximations only holding locally). The authors should reflect on how these assumptions might be violated in practice and what the implications would be.
- The authors should reflect on the scope of the claims made, e.g., if the approach was only tested on a few datasets or with a few runs. In general, empirical results often depend on implicit assumptions, which should be articulated.
- The authors should reflect on the factors that influence the performance of the approach. For example, a facial recognition algorithm may perform poorly when image resolution is low or images are taken in low lighting. Or a speech-to-text system might not be used reliably to provide closed captions for online lectures because it fails to handle technical jargon.
- The authors should discuss the computational efficiency of the proposed algorithms and how they scale with dataset size.
- If applicable, the authors should discuss possible limitations of their approach to address problems of privacy and fairness.
- While the authors might fear that complete honesty about limitations might be used by reviewers as grounds for rejection, a worse outcome might be that reviewers discover limitations that aren't acknowledged in the paper. The authors should use their best judgment and recognize that individual actions in favor of transparency play an important role in developing norms that preserve the integrity of the community. Reviewers will be specifically instructed to not penalize honesty concerning limitations.

### 3. Theory Assumptions and Proofs

Question: For each theoretical result, does the paper provide the full set of assumptions and a complete (and correct) proof?

Answer: [NA]

Justification: The paper does not include theoretical results

Guidelines:

- The answer NA means that the paper does not include theoretical results.
- All the theorems, formulas, and proofs in the paper should be numbered and cross-referenced.
- All assumptions should be clearly stated or referenced in the statement of any theorems.
- The proofs can either appear in the main paper or the supplemental material, but if they appear in the supplemental material, the authors are encouraged to provide a short proof sketch to provide intuition.
- Inversely, any informal proof provided in the core of the paper should be complemented by formal proofs provided in appendix or supplemental material.
- Theorems and Lemmas that the proof relies upon should be properly referenced.

#### 4. Experimental Result Reproducibility

Question: Does the paper fully disclose all the information needed to reproduce the main experimental results of the paper to the extent that it affects the main claims and/or conclusions of the paper (regardless of whether the code and data are provided or not)?

Answer: [Yes]

Justification: The paper discloses the main implementation details in the main body, and additional details in the appendix. We will release the code, model, and new datasets for reproducibility.

Guidelines:

- The answer NA means that the paper does not include experiments.
- If the paper includes experiments, a No answer to this question will not be perceived well by the reviewers: Making the paper reproducible is important, regardless of whether the code and data are provided or not.
- If the contribution is a dataset and/or model, the authors should describe the steps taken to make their results reproducible or verifiable.
- Depending on the contribution, reproducibility can be accomplished in various ways. For example, if the contribution is a novel architecture, describing the architecture fully might suffice, or if the contribution is a specific model and empirical evaluation, it may be necessary to either make it possible for others to replicate the model with the same dataset, or provide access to the model. In general, releasing code and data is often one good way to accomplish this, but reproducibility can also be provided via detailed instructions for how to replicate the results, access to a hosted model (e.g., in the case of a large language model), releasing of a model checkpoint, or other means that are appropriate to the research performed.
- While NeurIPS does not require releasing code, the conference does require all submissions to provide some reasonable avenue for reproducibility, which may depend on the nature of the contribution. For example
  - (a) If the contribution is primarily a new algorithm, the paper should make it clear how to reproduce that algorithm.
  - (b) If the contribution is primarily a new model architecture, the paper should describe the architecture clearly and fully.
  - (c) If the contribution is a new model (e.g., a large language model), then there should either be a way to access this model for reproducing the results or a way to reproduce the model (e.g., with an open-source dataset or instructions for how to construct the dataset).
  - (d) We recognize that reproducibility may be tricky in some cases, in which case authors are welcome to describe the particular way they provide for reproducibility. In the case of closed-source models, it may be that access to the model is limited in some way (e.g., to registered users), but it should be possible for other researchers to have some path to reproducing or verifying the results.

#### 5. Open access to data and code

Question: Does the paper provide open access to the data and code, with sufficient instructions to faithfully reproduce the main experimental results, as described in supplemental material?

Answer: **[Yes]**

Justification: We will publicly release the code, model, and datasets after review.

Guidelines:

- The answer NA means that paper does not include experiments requiring code.
- Please see the NeurIPS code and data submission guidelines (<https://nips.cc/public/guides/CodeSubmissionPolicy>) for more details.
- While we encourage the release of code and data, we understand that this might not be possible, so “No” is an acceptable answer. Papers cannot be rejected simply for not including code, unless this is central to the contribution (e.g., for a new open-source benchmark).
- The instructions should contain the exact command and environment needed to run to reproduce the results. See the NeurIPS code and data submission guidelines (<https://nips.cc/public/guides/CodeSubmissionPolicy>) for more details.
- The authors should provide instructions on data access and preparation, including how to access the raw data, preprocessed data, intermediate data, and generated data, etc.
- The authors should provide scripts to reproduce all experimental results for the new proposed method and baselines. If only a subset of experiments are reproducible, they should state which ones are omitted from the script and why.
- At submission time, to preserve anonymity, the authors should release anonymized versions (if applicable).
- Providing as much information as possible in supplemental material (appended to the paper) is recommended, but including URLs to data and code is permitted.

## 6. Experimental Setting/Details

Question: Does the paper specify all the training and test details (e.g., data splits, hyper-parameters, how they were chosen, type of optimizer, etc.) necessary to understand the results?

Answer: **[Yes]**

Justification: The paper discloses the main implementation details in the main body, and additional details in the appendix.

Guidelines:

- The answer NA means that the paper does not include experiments.
- The experimental setting should be presented in the core of the paper to a level of detail that is necessary to appreciate the results and make sense of them.
- The full details can be provided either with the code, in appendix, or as supplemental material.

## 7. Experiment Statistical Significance

Question: Does the paper report error bars suitably and correctly defined or other appropriate information about the statistical significance of the experiments?

Answer: **[No]**

Justification: We don't have enough resources and time to repeat experiments and report error bars for different initialization conditions.

Guidelines:

- The answer NA means that the paper does not include experiments.
- The authors should answer “Yes” if the results are accompanied by error bars, confidence intervals, or statistical significance tests, at least for the experiments that support the main claims of the paper.
- The factors of variability that the error bars are capturing should be clearly stated (for example, train/test split, initialization, random drawing of some parameter, or overall run with given experimental conditions).

- The method for calculating the error bars should be explained (closed form formula, call to a library function, bootstrap, etc.)
- The assumptions made should be given (e.g., Normally distributed errors).
- It should be clear whether the error bar is the standard deviation or the standard error of the mean.
- It is OK to report 1-sigma error bars, but one should state it. The authors should preferably report a 2-sigma error bar than state that they have a 96% CI, if the hypothesis of Normality of errors is not verified.
- For asymmetric distributions, the authors should be careful not to show in tables or figures symmetric error bars that would yield results that are out of range (e.g. negative error rates).
- If error bars are reported in tables or plots, The authors should explain in the text how they were calculated and reference the corresponding figures or tables in the text.

## 8. Experiments Compute Resources

Question: For each experiment, does the paper provide sufficient information on the computer resources (type of compute workers, memory, time of execution) needed to reproduce the experiments?

Answer: **[Yes]**

Justification: We disclose the computer resources and the number of training steps.

Guidelines:

- The answer NA means that the paper does not include experiments.
- The paper should indicate the type of compute workers CPU or GPU, internal cluster, or cloud provider, including relevant memory and storage.
- The paper should provide the amount of compute required for each of the individual experimental runs as well as estimate the total compute.
- The paper should disclose whether the full research project required more compute than the experiments reported in the paper (e.g., preliminary or failed experiments that didn't make it into the paper).

## 9. Code Of Ethics

Question: Does the research conducted in the paper conform, in every respect, with the NeurIPS Code of Ethics <https://neurips.cc/public/EthicsGuidelines>?

Answer: **[Yes]**

Justification: We conduct research with the NeurIPS Code of Ethics.

Guidelines:

- The answer NA means that the authors have not reviewed the NeurIPS Code of Ethics.
- If the authors answer No, they should explain the special circumstances that require a deviation from the Code of Ethics.
- The authors should make sure to preserve anonymity (e.g., if there is a special consideration due to laws or regulations in their jurisdiction).

## 10. Broader Impacts

Question: Does the paper discuss both potential positive societal impacts and negative societal impacts of the work performed?

Answer: **[Yes]**

Justification: We discuss the potential societal impacts in the conclusions.

Guidelines:

- The answer NA means that there is no societal impact of the work performed.
- If the authors answer NA or No, they should explain why their work has no societal impact or why the paper does not address societal impact.
- Examples of negative societal impacts include potential malicious or unintended uses (e.g., disinformation, generating fake profiles, surveillance), fairness considerations (e.g., deployment of technologies that could make decisions that unfairly impact specific groups), privacy considerations, and security considerations.

- The conference expects that many papers will be foundational research and not tied to particular applications, let alone deployments. However, if there is a direct path to any negative applications, the authors should point it out. For example, it is legitimate to point out that an improvement in the quality of generative models could be used to generate deepfakes for disinformation. On the other hand, it is not needed to point out that a generic algorithm for optimizing neural networks could enable people to train models that generate Deepfakes faster.
- The authors should consider possible harms that could arise when the technology is being used as intended and functioning correctly, harms that could arise when the technology is being used as intended but gives incorrect results, and harms following from (intentional or unintentional) misuse of the technology.
- If there are negative societal impacts, the authors could also discuss possible mitigation strategies (e.g., gated release of models, providing defenses in addition to attacks, mechanisms for monitoring misuse, mechanisms to monitor how a system learns from feedback over time, improving the efficiency and accessibility of ML).

## 11. Safeguards

Question: Does the paper describe safeguards that have been put in place for responsible release of data or models that have a high risk for misuse (e.g., pretrained language models, image generators, or scraped datasets)?

Answer: **[Yes]**

Justification: The dataset will be released with safeguards.

Guidelines:

- The answer NA means that the paper poses no such risks.
- Released models that have a high risk for misuse or dual-use should be released with necessary safeguards to allow for controlled use of the model, for example by requiring that users adhere to usage guidelines or restrictions to access the model or implementing safety filters.
- Datasets that have been scraped from the Internet could pose safety risks. The authors should describe how they avoided releasing unsafe images.
- We recognize that providing effective safeguards is challenging, and many papers do not require this, but we encourage authors to take this into account and make a best faith effort.

## 12. Licenses for existing assets

Question: Are the creators or original owners of assets (e.g., code, data, models), used in the paper, properly credited and are the license and terms of use explicitly mentioned and properly respected?

Answer: **[Yes]**

Justification: We have inspected and followed the requirements of the licenses of assets.

Guidelines:

- The answer NA means that the paper does not use existing assets.
- The authors should cite the original paper that produced the code package or dataset.
- The authors should state which version of the asset is used and, if possible, include a URL.
- The name of the license (e.g., CC-BY 4.0) should be included for each asset.
- For scraped data from a particular source (e.g., website), the copyright and terms of service of that source should be provided.
- If assets are released, the license, copyright information, and terms of use in the package should be provided. For popular datasets, [paperswithcode.com/datasets](https://paperswithcode.com/datasets) has curated licenses for some datasets. Their licensing guide can help determine the license of a dataset.
- For existing datasets that are re-packaged, both the original license and the license of the derived asset (if it has changed) should be provided.

- If this information is not available online, the authors are encouraged to reach out to the asset's creators.

### 13. New Assets

Question: Are new assets introduced in the paper well documented and is the documentation provided alongside the assets?

Answer: [Yes]

Justification: We introduce new datasets and describe the details in the main body and appendix.

Guidelines:

- The answer NA means that the paper does not release new assets.
- Researchers should communicate the details of the dataset/code/model as part of their submissions via structured templates. This includes details about training, license, limitations, etc.
- The paper should discuss whether and how consent was obtained from people whose asset is used.
- At submission time, remember to anonymize your assets (if applicable). You can either create an anonymized URL or include an anonymized zip file.

### 14. Crowdsourcing and Research with Human Subjects

Question: For crowdsourcing experiments and research with human subjects, does the paper include the full text of instructions given to participants and screenshots, if applicable, as well as details about compensation (if any)?

Answer: [NA]

Justification: The paper does not involve crowdsourcing nor research with human subjects.

Guidelines:

- The answer NA means that the paper does not involve crowdsourcing nor research with human subjects.
- Including this information in the supplemental material is fine, but if the main contribution of the paper involves human subjects, then as much detail as possible should be included in the main paper.
- According to the NeurIPS Code of Ethics, workers involved in data collection, curation, or other labor should be paid at least the minimum wage in the country of the data collector.

### 15. Institutional Review Board (IRB) Approvals or Equivalent for Research with Human Subjects

Question: Does the paper describe potential risks incurred by study participants, whether such risks were disclosed to the subjects, and whether Institutional Review Board (IRB) approvals (or an equivalent approval/review based on the requirements of your country or institution) were obtained?

Answer: [NA]

Justification: The paper does not involve crowdsourcing nor research with human subjects.

Guidelines:

- The answer NA means that the paper does not involve crowdsourcing nor research with human subjects.
- Depending on the country in which research is conducted, IRB approval (or equivalent) may be required for any human subjects research. If you obtained IRB approval, you should clearly state this in the paper.
- We recognize that the procedures for this may vary significantly between institutions and locations, and we expect authors to adhere to the NeurIPS Code of Ethics and the guidelines for their institution.
- For initial submissions, do not include any information that would break anonymity (if applicable), such as the institution conducting the review.

## A Satellite-Aerial Dataset Collection Process

Our data collection process involves the following steps: (1) deploying UAVs over selected areas to capture thermal image patches embedded with GPS metadata; (2) generating a unified thermal orthomosaic<sup>1</sup>; (3) cropping and aligning corresponding regions from satellite imagery with a spatial resolution of 1m/pixel; (4) excluding regions with invalid thermal data; and (5) applying grid sampling to extract square image patches for model training and evaluation (following the setup in [57], we adopt a sampling stride of 35m and a crop size of  $512 \times 512$ ). This process ensures the precise alignment between satellite RGB and thermal images.

## B Dataset Preprocessing Details

For large-scale training, all datasets are converted into the WebDataset<sup>2</sup> format, except for the satellite-aerial datasets. These datasets consist of paired, spatially aligned thermal and satellite RGB maps, from which we randomly sample regions across the entire map. We also detail the specific preprocessing steps applied to each dataset to ensure reproducibility:

- **NII-CU:** Resized RGB images to match thermal image dimensions.
- **TARDAL:** Created an 80%/20% train/test split by random sampling since no official split was provided in the dataset.
- **Freiburg:** Removed the black padding from thermal images on both right and left sizes.

## C Additional Training Details

We conduct all training and evaluation using a single NVIDIA A100 or H100 GPU. For training the thermal encoder and decoder, we employ a batch size of 16 and use the AdamW [33] optimizer with a learning rate of  $6 \times 10^{-5}$  and a weight decay of  $1 \times 10^{-3}$ , over a total of 200k training steps. All other configurations follow the default settings of the Latent Diffusion Model [39]. In training the flow-based generative models, we use a batch size of 64 with AdamW optimizer at a learning rate of  $1 \times 10^{-4}$  and no weight decay, for 200k training steps.

## D Dataset Parameters Comparison

A comparison between the Boson-night dataset [57] and our datasets is provided in Table 6, highlighting our contributions in terms of broader geographic coverage, increased diversity of thermal sensors, and the inclusion of both daytime and nighttime imagery.

Table 6: **Comparison of dataset parameters between Boson-night [57] and our datasets.** The differences are highlighted regarding area coverage, satellite map sources, thermal sensors used, collection years, and the number of surveyed regions.

Dataset Name	Area	Satellite Map	Thermal Sensor	Collection Year	Number of Regions
Boson-night [57]	33km <sup>2</sup>	Bing	Boson	2021	1
DJI-day (Ours)	29km <sup>2</sup>	ESRI <sup>3</sup>	DJI Zenmuse H20T	2023	1
Bosonplus-day (Ours)	85km <sup>2</sup>	ESRI <sup>3</sup>	Bosonplus	2024	3 <sup>4</sup>
Bosonplus-night (Ours)	94km <sup>2</sup>	ESRI <sup>3</sup>	Bosonplus	2024	3 <sup>4</sup>

## E Thermal Auto-encoder Training Details and Reconstruction Performance

This section details the training procedure and reconstruction performance of the thermal encoder  $E_T$  and decoder  $D_T$ . Both components are trained using the KL-VAE framework [39] on our curated

<sup>1</sup>We used Agisoft Metashape to generate the orthomosaic: <https://www.agisoft.com/>

<sup>2</sup><https://github.com/webdataset/webdataset>

<sup>3</sup>ESRI satellite map: <https://www.esri.com/en-us/home>

<sup>4</sup>For compliance, we will release data only for 2 regions in Bosonplus-day and Bosonplus-night.

Table 7: Reconstruction FID and PSNR performance across multiple RGB-T datasets

Method	FLIR	LLVIP	AVIID	MSRS	NII-CU	M <sup>3</sup> FD	Bosonplus-day	Bosonplus-night	Boson-night
FID ↓									
klvae w/o GAN loss	18.51	2.94	18.16	14.37	9.07	5.50	16.63	6.48	4.24
klvae w/ GAN loss	14.66	3.14	12.21	12.20	8.67	5.33	6.73	3.52	2.00
PSNR ↑									
klvae w/o GAN loss	30.10	37.63	31.29	38.73	45.73	40.12	30.46	41.32	43.53
klvae w/ GAN loss	28.74	36.59	30.07	37.60	45.24	39.03	29.15	40.84	43.16

Table 8: Style vs. CLIP Embeddings in ThermalGen.

Method	Bosonplus-day ↓	Bosonplus-night ↓	FLIR ↓
ThermalGen (Style embedding)	76.91	75.80	70.09
ThermalGen (CLIP embedding)	106.08	89.65	75.49

RGB-T dataset collection, optimized with a combination of reconstruction losses (L1 and LPIPS [60]) and KL regularization on the latent space. After 300 epochs (200k steps) of training, we optionally fine-tune the final decoder layers for 75 epochs using a GAN loss plus the loss mentioned above, as in the original LDM [39], to enhance FID scores without altering the latent representation, but it will slightly negatively affect PSNR metrics. We note that the results reported in the paper use the decoder **without** GAN loss.

## F Comparison of Style and CLIP Embeddings

We compare ThermalGen with two embedding strategies: (1) fixed style embeddings and (2) CLIP-based embeddings extracted from paired RGB images. As shown in Table 8, fixed style embeddings yield substantially lower FID scores on the Bosonplus-day and Bosonplus-night datasets, while achieving comparable performance on FLIR. Moreover, using fixed style embeddings improves computational efficiency by removing the need to compute CLIP features, demonstrating both the effectiveness and efficiency of our approach.

## G Evaluation Dataset Comparison

We provide a detailed comparison of the evaluation datasets in Table 9, organized by key sources of variation. To further illustrate domain differences, we present t-SNE visualizations of thermal features in Fig. 8 extracted using DINOv2 for the following dataset pairs: *Bosonplus-night* vs. *Boson-night* (sensor variation), *Bosonplus-day* vs. *AVIID* (viewpoint variation), and *Bosonplus-day* vs. *Bosonplus-night* (diurnal variation). These analyses reveal significant feature discrepancies across conditions, while demonstrating that our model effectively adapts to such shifts.

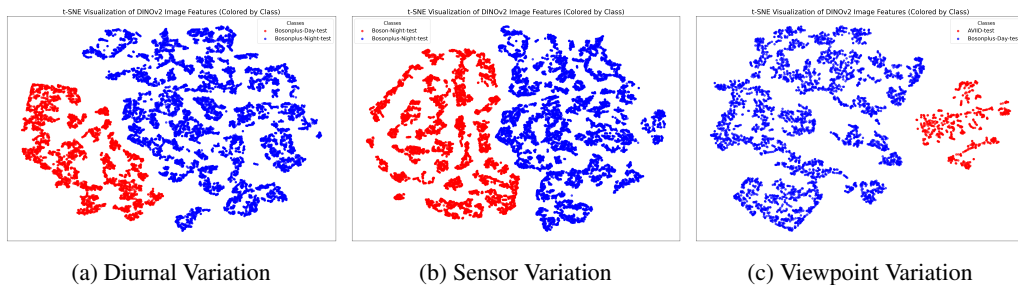


Figure 8: t-SNE Analysis for Diurnal, Sensor, and Viewpoint Variation of Datasets

Table 9: **Evaluation Dataset Attribute Comparison.** Attributes include diurnal setting, thermal sensor configuration, viewpoint, and environment type.

Dataset	Diurnal	Sensor Configuration	Viewpoint	Environment
Boson-night	Night	FLIR Boson	Satellite-aerial	Wild
Bosonplus-day	Day	FLIR Bosonplus	Satellite-aerial	Wild
Bosonplus-night	Night	FLIR Bosonplus	Satellite-aerial	Wild
LLVIP	Day/Night	Vanadium Oxide Uncooled Focal Plane Arrays	Aerial	Urban
NII-CU	Day	FLIR Vue Pro	Aerial	Wild
AVIID	Day/Night	Infrared (640×480, 8–14 $\mu$ m)	Aerial	Urban
M3FD	Day/Night	Infrared (640×512, 8–14 $\mu$ m)	Ground	Diverse
MSRS	Day/Night	InfRec R500	Ground	Urban
FLIR	Day/Night	FLIR Tau 2	Ground	Urban